



# Effects of hydrofluoric acid pre-deashing of rice husk on physicochemical properties and CO<sub>2</sub> adsorption performance of nitrogen-enriched biochar



Xiong Zhang, Shihong Zhang, Haiping Yang, Jingai Shao, Yingquan Chen, Ye Feng, Xianhua Wang\*, Hanping Chen

State Key Laboratory of Coal Combustion, Huazhong University of Science and Technology, Wuhan 430074, Hubei Province, China

## ARTICLE INFO

### Article history:

Received 25 May 2015

Received in revised form

10 August 2015

Accepted 16 August 2015

Available online 24 September 2015

### Keywords:

Deashing

Rice husk

Biochar

High-temperature ammonia treatment

CO<sub>2</sub> adsorption

## ABSTRACT

In order to enhance CO<sub>2</sub> adsorption capacity of rice husk char, raw rice husk was pre-deashed by HF (hydrofluoric acid) and used as precursor for preparing nitrogen-enriched biochar with high temperature ammonia treatment in this work. The effects of rice husk pre-deashing on the physicochemical properties and CO<sub>2</sub> adsorption performance of nitrogen-enriched biochar were investigated. The results show that the micropore surface area of the nitrogen-enriched biochar derived from pre-deashed rice husk (labeled as HF-N-Char) is 545.74 m<sup>2</sup>/g, more than that of the nitrogen-enriched biochar derived from raw rice husk (labeled as N-Char, and its micropore surface area is 303.10 m<sup>2</sup>/g). The nitrogen content of HF-N-Char is 2.53 wt%, much higher than that of N-Char (1.64 wt%). It indicates that the deashing treatment not only improves the pore structure of nitrogen-enriched biochar, but also enhances the introduction of nitrogen-containing functional groups. In addition, the CO<sub>2</sub> adsorption capacity of HF-N-Char (77.9 mg/g at 30 °C and 18.1 mg/g at 120 °C) is larger than that of N-Char (59.5 mg/g at 30 °C and 15.1 mg/g at 120 °C). The results may be helpful for the development of novel cost-effective CO<sub>2</sub> adsorbents.

© 2015 Elsevier Ltd. All rights reserved.

## 1. Introduction

Global warming is commonly considered as the result of sharp increase in GHG (greenhouse gas) concentration in the atmosphere [1]. CO<sub>2</sub> is estimated to contribute up to 60% of total anthropogenic GHG emissions [2]; to this effect, reducing CO<sub>2</sub> emissions is paramount to successfully mitigating global warming. CCUS (CO<sub>2</sub> Capture, Utilization and Storage) technology is an important and widely researched method of reducing CO<sub>2</sub> emissions without influencing energy supply or energy structure [3]. CO<sub>2</sub> capture (namely, separating CO<sub>2</sub> from flue gasses) is a key but also very expensive step in CCUS implementation [4]. Among various CO<sub>2</sub> separation technologies, such as adsorption [5–10], absorption [11,12], cryogenic distillation [13], and membrane separation [14,15], adsorption is one of the most appealing technology to realize large-scale CO<sub>2</sub> capture due to its low energy

requirement, cost-effectiveness, simple operation, and adaptability over a relatively wide range of temperatures and pressures [16].

Appropriate selection of adsorbents is vital to successful adsorption technology. Activated carbon has long been utilized as a commercial adsorbent, favored for its excellent porous structures and abundant surface functional groups [17]. However, traditional activated carbon is made of coal [18], thus expensive raw materials and laborious manufacturing process prevent its use as a large-scale CO<sub>2</sub> capture material [19]. Biochar, derived from biomass, is similar to activated carbon in microstructure, but more eco-friendly, cheaper, and with abundant precursor resources [7,9,20]. Despite these advantages, the textural characteristics and surface chemical properties of biochars, two factors responsible for overall adsorbent performance [21,22], are poorer than commercial activated carbon [17]. Modifying biochars to improve their textural characteristics and surface chemical properties is urgently necessary to improve biochar adsorption performance and promote the material's wider utilization.

\* Corresponding author. 1037 Luoyu Road, Wuhan, Hubei, China. Tel.: +86 27 87542417; fax: +86 27 87545526.

E-mail address: [wxxwhhy@sina.com](mailto:wxxwhhy@sina.com) (X. Wang).

In a previous study conducted by this research team [23], it was discovered that high-temperature ammonia treatment (also referred to as “ammonification”) not only effectively introduces nitrogen functional groups onto the carbon surface, but also successfully improves micropore structure. Previous studies [6–9,16] on the ammonification of biochars focused primarily on the effects of modification conditions on biochars, such as temperature, ammonia concentration, and modification time. The effects of ash in precursors on ammonification treatment must also be studied carefully, because ash in precursors plays an important role during biochar preparation by influencing the transformation of physicochemical properties.

In one previous study, Das et al. [24] investigated the influence of deashing pretreatment on the pyrolysis of sugarcane bagasse, and results showed that HF (hydrofluoric acid) deashing and HCl (hydrochloric acid) deashing both significantly increased the BET (Brunauer–Emmett–Teller) surface area of the derived biochars, because acid wash promoted the decomposition and dissolution of minerals in precursors, which was beneficial to the development of porous structure. The BET surface area of HF-treated bagasse pyrolysis char was 242.73 m<sup>2</sup>/g, and that of HCl-treated bagasse pyrolysis char was 153.72 m<sup>2</sup>/g, while that of untreated bagasse pyrolysis char is only 98 m<sup>2</sup>/g. Deashing by HF showed much better performance than deashing by HCl. In another relevant study, Basta et al. [25] investigated the effects of deashing on rice-straw-derived biochars. Their results showed that deashing successfully improved the adsorption capacities of biochars modified by KOH, while deashing did not significantly improve the adsorption properties of biochars modified by H<sub>3</sub>PO<sub>4</sub>. It can be inferred that the impact of precursor deashing on the properties of resultant biochars is closely related to the modification medium. Nevertheless, how precursor deashing affects the physicochemical properties of biochars under high-temperature ammonia treatment remains unclear.

The primary object of this study is to investigate the impact of deashing pretreatment on biochars modified by high-temperature ammonia treatment. Rice husk with high ash content was chosen as raw material, and was deashed by HF solution before pyrolysis. The deashed rice husk and raw rice husk were pyrolyzed and treated with ammonia under the same conditions to obtain biochar samples. The physicochemical properties and CO<sub>2</sub> adsorption performance of the derived biochars were then analyzed and compared. Some interesting results were obtained, which may be helpful for preparing high-performance biochars in the future, as well as promoting the utilization of biochars in CO<sub>2</sub> separation systems.

## 2. Materials and methods

### 2.1. Materials

The raw rice husk used to prepare biochars was collected from Wuhan, China. Specifications of the raw RH (rice husk) are shown in Table 1. The material was first dried at 50 °C for 12 h, then crushed and sieved to obtain particles ranging from 0.1 to 1 mm in size.

**Table 1**  
The proximate and ultimate analysis result of rice husk.

Sample	Ultimate analysis (ad. wt.%)				
	C	H	N	S	O <sup>a</sup>
RH	42.04	5.28	0.38	0.17	30.64

<sup>a</sup> Calculated by difference. RH represents raw rice husk.

### 2.2. Deashing pretreatment

Acid washing was performed to remove mineral matter from the rice husk by mixing 30 ml HF (40%), 60 ml deionized water, and 25 g raw material in a Teflon wide-mouth bottle. The mixture was stirred at 60 °C for 24 h and filtered in a Teflon funnel using specialized ash-less filter paper, then washed with distilled water until pH reached 7. The deashed material was then dried in an oven at 50 °C and kept in a tightly closed screw cap bottle. The deashed sample was labeled “HF-RH”.

### 2.3. Ash characteristics

Proximate analysis was used to determine ash content. To analyze the ash composition of RH and HF-RH, the samples were burnt into ash at 600 °C (referring to Standard ASTM E-1755-01.) Ash composition was analyzed with an XRF (X-ray fluorescence) instrument (EAGLE III, EDAX Inc., USA). Three scanning points were analyzed to obtain an average value, in order to minimize error.

### 2.4. Preparation of biochars

3 g RH/HF-RH sample was placed in a fixed bed reactor and heated at 10 °C/min up to the final pyrolysis temperature of 600 °C, then kept for 30 min in an N<sub>2</sub> atmosphere (N<sub>2</sub> = 400 ml/min). The sample was then heated at 10 °C/min up to the final modification temperature of 700 °C. Upon reaching the preset temperature, the atmosphere was switched to a mixture of N<sub>2</sub> and NH<sub>3</sub> (N<sub>2</sub> = 400 ml/min, NH<sub>3</sub> = 80 ml/min), and held for 30 min. Once the ammonification process was complete, the vertical heater was shut down and the biochar as-derived was cooled in an N<sub>2</sub> atmosphere. The above conditions (referred to as one-step ammonification) were identified in our previous study as optimal for pore structure improvement while simultaneously ensuring that nitrogen functional groups do not break down [23]. The obtained nitrogen-enriched biochars from RH and HF-RH were labeled “N-Char” and “HF-N-Char”, respectively. The raw RH sample was also pyrolyzed under the same conditions without the ammonification treatment as a control, labeled “R-Char”.

### 2.5. Physical and chemical properties

The impact of acid washing on the surface characteristics of RH, HF-RH, and HF-N-Char was investigated by FESEM (field emission scanning electron microscopy, Sirion 200, FEI, Holland). Surface elemental analysis of samples was conducted by EDX (energy dispersive X-ray spectroscopy, EDAX Inc., USA) to ascertain the involvement of superficial element distribution.

To explore the effects of deashing treatment on the textural formation of the derived biochars, the surface area and pore structure characteristics of all precursors and biochars were determined from N<sub>2</sub> and CO<sub>2</sub> adsorption isotherms obtained at 77 K and 273 K using automatic adsorption equipment (ASAP2020, Micromeritics, USA). The BET surface area ( $S_{\text{BET}}$ ), micropore surface area ( $S_{\text{mic}}$ ), and micropore volume ( $V_{\text{mic}}$ ) of samples were calculated according to the BET equation and the DR (Dubinin–Radushkevich) equation. The distribution of micro-, meso- and macropores were analyzed according to DFT (density function theory). In this DFT approach, the local fluid density profile  $\rho(r)$  of the adsorbate at phase equilibrium is determined by minimization of the grand thermodynamic potential ( $\Omega$ ). The  $\Omega$  expressed as a function of the fluid density  $\rho(r)$  is given as [26]:

$$\Omega[\rho(r)] = F[\rho(r)] - \int \rho(r)[\mu - V_{ext}(r)] dr \quad (1)$$

where  $F[\rho(r)]$  is the intrinsic Helmholtz free energy functional,  $r$  is the spatial-coordinate,  $\mu$  is the chemical potential, and  $V_{ext}$  is potential imposed by the pore walls. The  $V_{ext}$  depends only on one spatial coordinate:

$$V_{ext}(z) = \phi_{sf}(z) + \phi_{sf}(H - z) \quad (2)$$

where  $\phi_{sf}$  is the adsorbate-bounding slabs potential,  $H$  is physical pore width of adsorbent and  $z$  is the distance between the adsorbate and the adsorbent surface. The pore size distribution can be calculated by an adsorption isotherm  $N(P, H)$ :

$$N(P, H) = \frac{1}{H} \int_0^H [\rho(z) - \rho_b] dz \quad (3)$$

where  $\rho_b$  is bulk gas density and  $P$  is pressure.

To analyze changes in surface functional groups, the surface chemical properties of all samples were investigated by FTIR (Fourier transform infrared spectroscopy). Carbon and nitrogen contents were measured with a CHNS elementary analyzer (Vario Micro Cube, Germany).

## 2.6. CO<sub>2</sub> adsorption

The CO<sub>2</sub> adsorption performance of biochars was characterized by adsorbing CO<sub>2</sub> in a fix bed reactor with a TGA (thermogravimetric analyzer). The experimental procedure (shown in Fig. 1), step-by-step, was conducted as follows [7]:

Step 1: About 10 mg of each sample was loaded in a small pan and heated up to 200 °C under an N<sub>2</sub> atmosphere (100 ml/min) and held isothermally for 1 h to remove moisture and other gases.

Step 2: Heating stopped until the temperature decreased to the targeted adsorption temperature of 30 °C/120 °C. Once reaching the targeted temperature, the atmosphere was switched to pure CO<sub>2</sub> (100 ml/min) and the sample was held isothermally for 1 h to ensure that the adsorption process had finished. The weight increase during this stage was considered the total CO<sub>2</sub> adsorption amount.

Step 3: The CO<sub>2</sub> atmosphere was switched to an N<sub>2</sub> atmosphere while temperature was increased at a heating rate of 10 °C/min to 200 °C, then held isothermally for 1 h to realize desorption of CO<sub>2</sub>. At this point, one adsorption–desorption circle was complete.

To investigate the recoverability of the biochars, three adsorption–desorption cycles were conducted by repeating the second and third steps.

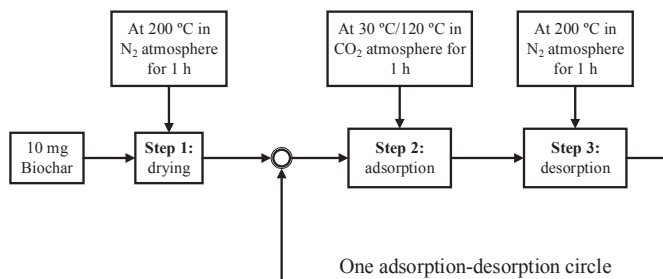


Fig. 1. CO<sub>2</sub> adsorption–desorption procedure.

## 3. Results and discussion

### 3.1. Ash content and composition analysis

The proximate analysis and ash composition of RH and HF-RH are listed in Table 2 and Table 3, respectively. RH had a very high ash content, up to 15.96 wt.%, mainly comprised of SiO<sub>2</sub> (91.25 wt.%, Table 3). After washing by HF solution, the ash (A) content dramatically reduced to 0.94 wt.%, but the FC (fixed carbon) changed very little (from 11.03 wt.% to 10.83 wt.%). This implies that HF deashing treatment removed most of the raw ash. In addition, after deashing treatment, A/FC ratio likewise decreased from 1.45 to 0.087. The deashing efficiency of the HF solution reached 94.1%. Moisture content (M) also slightly decreased, while volatile content (V) quite dramatically increased (82.98 wt.%). This indicates that RH deashed by HF solution has high volatile content, which benefits the formation of pore structure during high-temperature treatment process [27].

Table 3 shows where SiO<sub>2</sub> and K<sub>2</sub>O content in the samples both decreased significantly, while MgO, CaO, and Fe<sub>2</sub>O<sub>3</sub> considerably increased. Basically, the HF solution effectively removed Si and K, but not Mg, Ca, or Fe. The likely mechanism behind this is that compounds containing Si react with HF to form SiF<sub>4</sub>, while compounds containing Mg, Ca, and Fe tend to react with HF to form insoluble or just slightly soluble compounds; a similar mechanism exists for P and S. The most likely reaction mechanisms can be expressed as follows [28]:



### 3.2. Textural characterization

#### 3.2.1. FESEM analysis

Fig. 2 shows FESEM images of RH, HF-RH and HF-N-Char. The main composition of a rice husk includes an outer epidermis, lower epidermis, and bundle of internal vascular tissues. The outer epidermis, as shown below, presents regular cone convex structure, with a bright and smooth surface (Fig. 2a). The vast majority of silicon content was concentrated on the surface, forming an Si-rich protective layer structure [29]. However, the embossed, relatively smooth surface of RH was replaced by a rougher surface

Table 2

The proximate analysis result of raw rice husk and the pre-deashed.

Sample	Proximate analysis (ad, wt.%)				A/FC
	M	V	A	FC	
RH	5.52	67.49	15.96	11.03	1.45
HF-RH	5.26	82.98	0.94	10.83	0.087

M, V, A and FC represent moisture, volatile, ash and fixed carbon, respectively. A/FC is the ratio of ash and fixed carbon. RH and HF-RH mean the raw rice husk and the pre-deashed, respectively.

**Table 3**  
XRF results of RH and HF-RH ashes.

Sample	Composition (wt.%)									
	MgO	Al <sub>2</sub> O <sub>3</sub>	SiO <sub>2</sub>	P <sub>2</sub> O <sub>5</sub>	SO <sub>3</sub>	Cl	K <sub>2</sub> O	CaO	MnO	Fe <sub>2</sub> O <sub>3</sub>
RH	0.48	1.03	91.25	0.75	1.17	0.61	2.56	1.62	0.19	0.34
HF-RH	3.56	1.68	2.07	3.16	35.24	1.26	0.72	47.57	0.55	4.18

after pre-deashing with HF solution (Fig. 2b). This phenomenon is attributable to the removal of mineral silicon and destruction of the protective layer, which, once disintegrated, exposed the internal xylem tissue and formed rougher morphology. The main framework of xylem and phloem tissues was barely affected after deashing treatment, however [25]. Fig. 2c shows FESEM images of HF-N-Char, where the original compact fibrous material turned into a much more porous carbon material with abundant tunnel-shaped pore structures after one-step ammonification. Removing the protective layer provided more opportunities for free radicals to pass through, and facilitated release of small molecular substances, which are altogether favorable for pore structure formation [27].

### 3.2.2. Pore distribution and surface area

Fig. 3 shows the N<sub>2</sub> and CO<sub>2</sub> adsorption isotherms of samples, respectively. The BET surface areas and the mesopore and macropore distribution of precursors and chars are calculated from the adsorption isotherms of N<sub>2</sub> at 77 K. The micropore properties (include S<sub>mic</sub>, V<sub>mic</sub> and micropore distribution) are determined by physical adsorption of CO<sub>2</sub> at 273 K. This is due to the existence of diffusion limitations to the entrance of N<sub>2</sub> molecule at 77 K in narrow micropores [20].

The BET surface area, micropore surface area, and micropore volume of all samples are presented in Table 4. The S<sub>BET</sub>, S<sub>mic</sub>, and V<sub>mic</sub> values of HF-RH are smaller than those of RH, suggesting that deashing blocked or collapsed the pores. Pore size distribution curves are displayed in Fig. 4, which clearly demonstrates the evolution of pore structure after pre-deashing treatment by HF solution. Mesopores and macropores significantly decreased after HF treatment, likely due to the removal of silicon promoting causing mesopores to overlap and form macropores, after which the excessive corrosion of HF collapsed the macropores [30]. In addition, the amount of narrow micropores (<0.7 nm) reduced considerably, but broader micropores (0.7–2 nm) slightly increased. The removal of inorganic minerals probably broadened the narrow micropores.

The S<sub>BET</sub> value of N-Char was smaller than that of R-Char, while the S<sub>mic</sub> and V<sub>mic</sub> values were larger (Table 4), implying that high-temperature ammonia treatment increased S<sub>mic</sub> and V<sub>mic</sub>, but

decreased S<sub>BET</sub>. Increases in S<sub>mic</sub> and V<sub>mic</sub> can be strictly attributed to the optimized micropore structure. Coincidentally, Fig. 5a shows that the micropore structure of N-Char is markedly better than that of R-Char. However, Fig. 5b shows where the narrow mesopores (2–7 nm) of N-Char had weaker structure than R-Char, but the structure of macropores and broad mesopores (7–50 nm) of N-Char are obviously more favorable than R-Char (Fig. 5b–c). It indicates that the influence of narrow mesopores on S<sub>BET</sub> was much greater than macropores or broad mesopores, because S<sub>BET</sub> is mainly dependent on mesopore and macropore structure [31].

Compared to R-Char and N-Char, HF-N-Char had maximum BET surface area, micropore surface area, and micropore volume (Table 4). The S<sub>BET</sub> value of HF-N-Char was 451.02 m<sup>2</sup>/g, an 85.3% and 89.7% increase, respectively, over R-char and N-Char. The S<sub>mic</sub> value of HF-N-Char was 545.74 m<sup>2</sup>/g, an 83.9% increase compared to R-char and 82.1% increase compared to N-Char. HF-N-Char's V<sub>mic</sub> was 0.219 ml/g, an 84.0% and 82.6% increase compared to R-char and N-Char, respectively. It can thus be concluded that deashing treatment led to obvious improvement of S<sub>BET</sub>, S<sub>mic</sub>, and V<sub>mic</sub> values. The pore structure in almost all size ranges of HF-N-Char was also the best of all samples (Fig. 5), indicating that pre-deashing not only eliminated the deterioration of narrow mesopores, but also intensified the enhancement of micropores and macropores during one-step ammonification process. The most likely mechanism for this is that Si removal decreased the formation of amorphous SiO<sub>2</sub> largely concentrated in the outer epidermis, and thus was disadvantageous to porous structure formation [29,30].

## 3.3. Chemical characterization

### 3.3.1. Elemental analysis

Surface elemental composition information for RH and HF-RH is listed in Table 5. The chemical composition of rice husk before and after deashing differed considerably. The surface Si<sup>s</sup> content decreased dramatically, from 43.71 wt.% to 0.19 wt.%, after deashing by HF solution; O<sup>s</sup> content increased from 33.86 wt.% to 38.53 wt.% and N<sup>s</sup> from 2.28 wt.% to 3.2 wt.%. Table 6 shows where the change trend of the surface atomic C<sup>a</sup>, N<sup>a</sup>, and Si<sup>a</sup> were the same as C<sup>s</sup>, N<sup>s</sup>, and Si<sup>s</sup>. However, the surface atomic ratio of Si<sup>a</sup>/C<sup>a</sup> decreased from

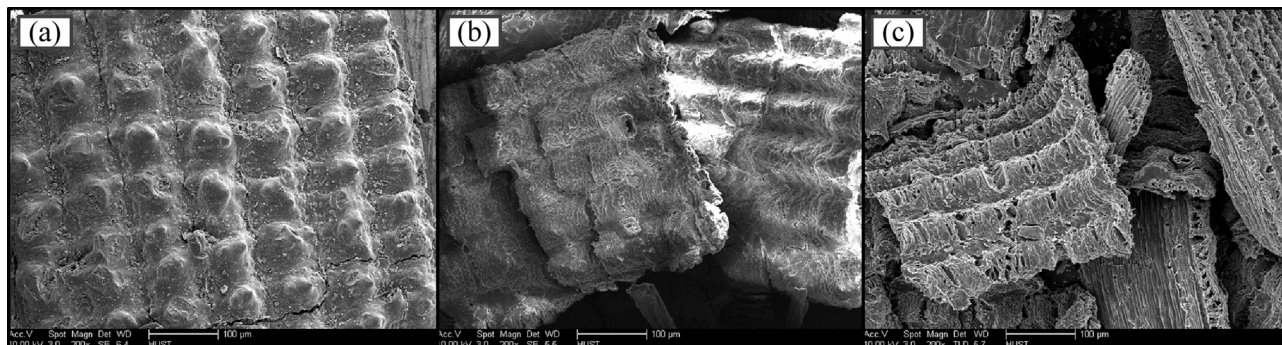


**Fig. 2.** FESEM micrographs of RH (a, 200 $\times$ , 100  $\mu$ m), HF-RH (b, 200 $\times$ , 100  $\mu$ m) and HF-N-Char (c, 200 $\times$ , 100  $\mu$ m).

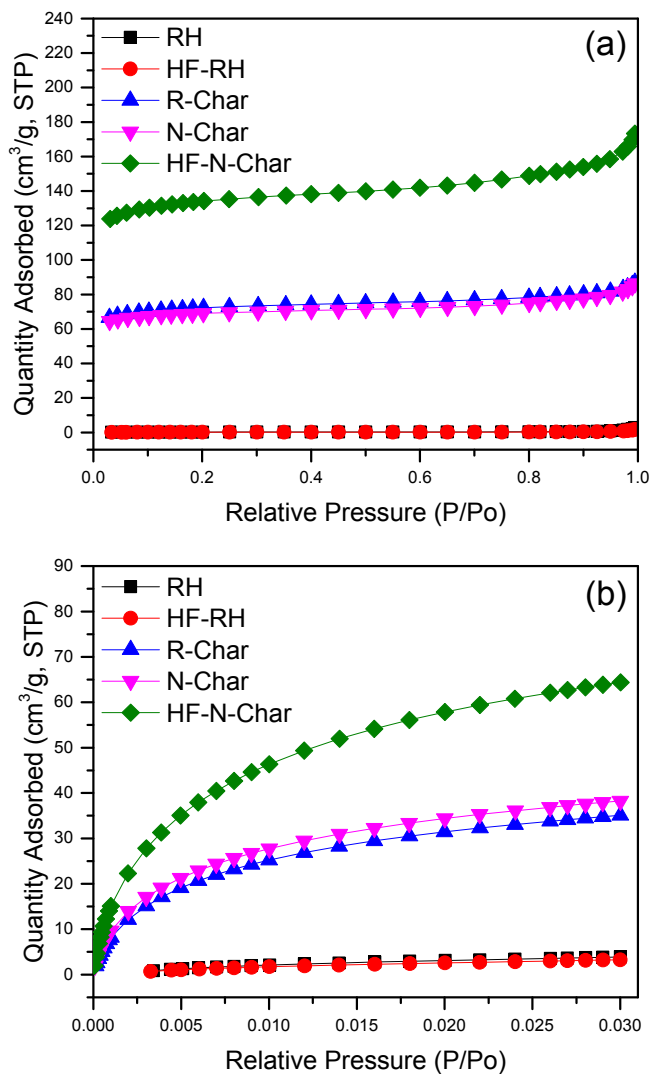


Fig. 3. The adsorption isotherms of prepared samples: (a) N<sub>2</sub> at 77 K and (b) CO<sub>2</sub> at 273 K.

0.99 to 0.0014, O<sup>a</sup>/C<sup>a</sup> decreased from 1.35 to 0.51, and N<sup>a</sup>/C<sup>a</sup> from 0.1 to 0.05, indicating that deashing treatment mainly removed Si, but less O and N – this explains the increased O<sup>s</sup> and N<sup>s</sup> content on the surface.

In addition, O<sup>a</sup> did not increase compared to O<sup>s</sup>, but decreased after deashing. Although the surface oxygen content increased, the surface oxygen atom content reduced, because the atomic mass constant of Si is larger than that of O. The surface O<sup>a</sup> represents the amount of surface oxygen functional groups, which are important active sites for the introduction of nitrogen functional groups, but not all of said oxygen functional groups form active sites [16,32]. Though the surface O<sup>a</sup> reduced after deashing, the nitrogen content

Table 4  
Physical properties and CN elementary analysis results.

Samples	S <sub>BET</sub> (m <sup>2</sup> /g)	S <sub>mic</sub> (m <sup>2</sup> /g)	V <sub>mic</sub> (ml/g)	C (wt.%)	N (wt.%)
RH	0.79	45.93	0.018	42.04	0.38
HF-RH	0.58	37.52	0.015	50.78	0.33
R-Char	243.06	296.69	0.119	52.62	0.52
N-Char	231.27	303.10	0.121	53.36	1.64
HF-N-Char	451.02	545.74	0.219	92.15	2.53

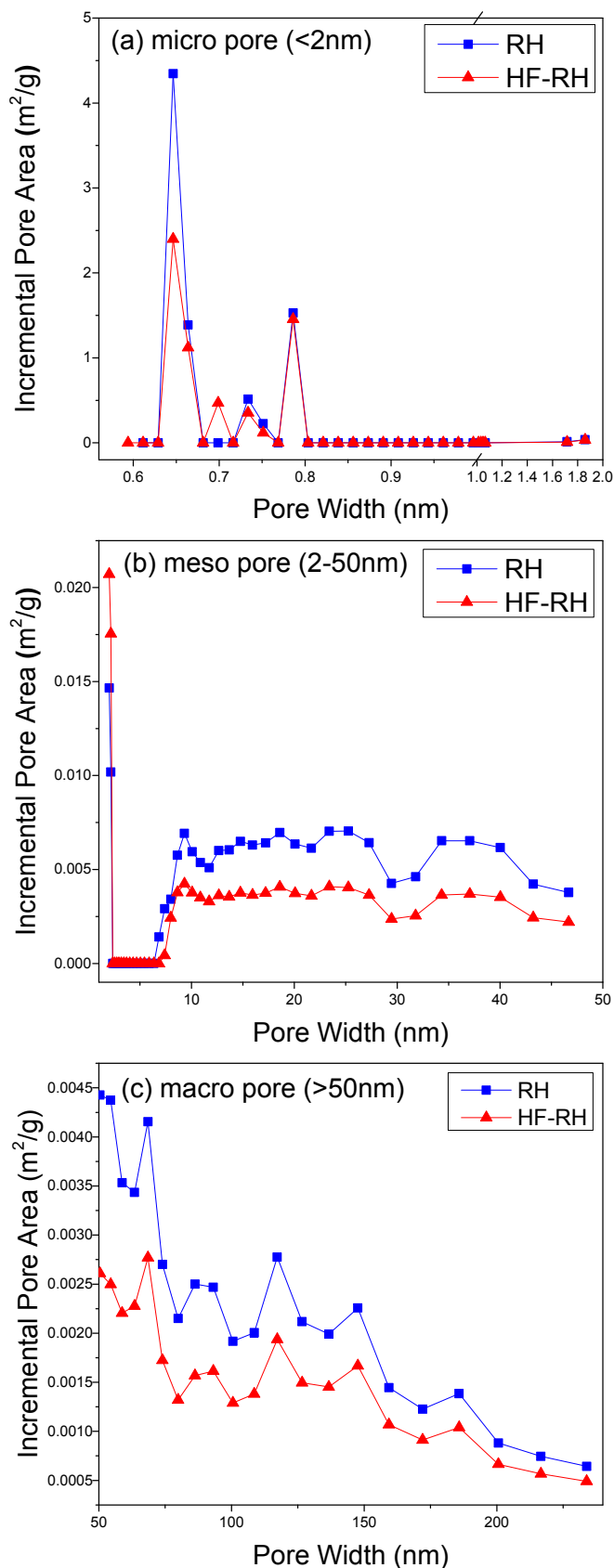


Fig. 4. The micro- (a), meso- (b), and macropores (c) distribution of RH and HF-RH.

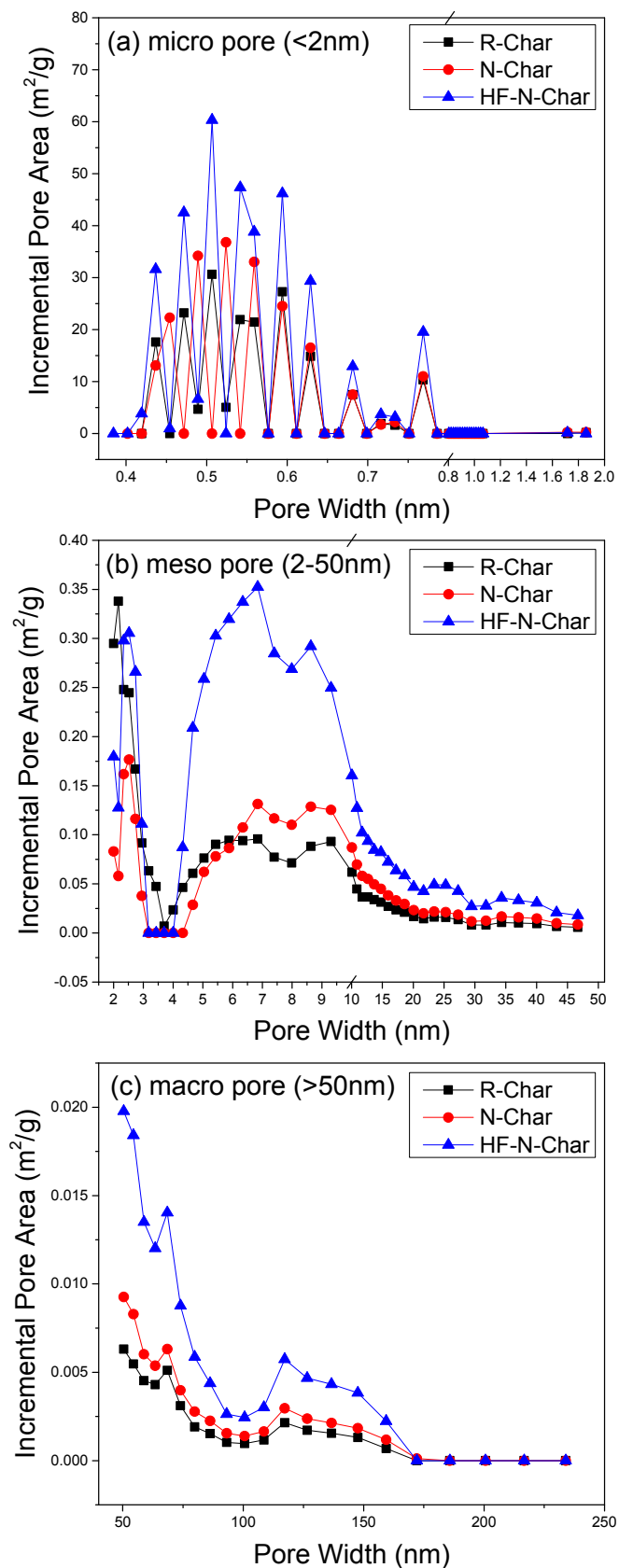


Fig. 5. The micro- (a), meso- (b), and macropores (c) distribution of R-char, N-Char and HF-N-Char.

of HF-N-Char was still greater than that of N-Char (Table 4). This illustrates that deashing treatment decreased the surface oxygen functional groups, but the number of available functional groups for the introduction of nitrogen functional groups increased.

The surface C<sup>s</sup> content of HF-N-Char was 89.95 wt.% (Table 5), which was lower than the total C content of 92.15 wt.% (Table 4). However, the surface N<sup>s</sup> content of HF-N-Char was 5.03 wt.%, which was more than the total N content (2.53 wt.%). The introduction of nitrogen functional groups increases surface N<sup>s</sup> content while reducing C<sup>s</sup> content [32].

### 3.3.2. Surface functional group analysis

The FTIR spectra of RH and HF-RH are illustrated in Fig. 6a, and those of R-Char, N-Char, and HF-N-Char are shown in Fig. 6b. The FTIR spectra of RH and HF-RH both demonstrate a broad peak centered at 3423 cm<sup>-1</sup>, which represents O–H stretching vibrations [8,20]. The broad peak of HF-RH is stronger than that of RH, indicating that the amount of O–H bonding in HF-RH was higher. The sharp peak at 1103 cm<sup>-1</sup> represents C–O–Si stretching vibrations, and the shorter peak at 796 cm<sup>-1</sup> can be assigned to Si–H stretching [30]. Both peaks of HF-RH are much weaker than those of RH, suggesting that HF treatment destroyed the C–O–Si and Si–H structures in RH.

The spectra of N-Char contains several peaks, which can be assigned to O–H stretching vibrations (at 3430 cm<sup>-1</sup>), aliphatic CH, CH<sub>2</sub>, and CH<sub>3</sub> asymmetric and symmetric stretching vibrations (at 2923 cm<sup>-1</sup> and 2860 cm<sup>-1</sup>) [8,32]. Most of these peaks practically disappear in the spectra of HF-N-Char, however, indicating that pre-deashing the rice husk promoted O–H and C–H breakage of the derived biochar. Conversely, the spectra of HF-N-Char demonstrates stronger peaks than N-Char at 1745 cm<sup>-1</sup>, 1571 cm<sup>-1</sup> and 1141 cm<sup>-1</sup>, representing N=O, pyridine C=N, and C–N stretching vibrations, respectively [9,23]. This shows that precursor pre-deashing increased the abundance of nitrogen-containing groups in the target biochar. The N content of HF-N-Char was the highest out of all samples (Table 4), further proving that pre-deashing rice husk promotes the introduction of N-containing functional groups during ammonification treatment. Pre-deashing with HF solution likely increased the amount of active sites on the char surface (in a similar manner as O–H), which benefits the introduction of nitrogen functional groups [32].

### 3.4. CO<sub>2</sub> adsorption

Fig. 7 depicts the CO<sub>2</sub> adsorption capacity and cyclic performance of R-char, N-Char, and HF-N-Char at 30 °C and 120 °C. It can be observed that compared with R-Char, when the adsorption temperature was 30 °C, the adsorption capacity of N-Char was 52.6 mg/g and had a slight increase, whereas the temperature increased to 120 °C, its adsorption capacity was 15.1 mg/g, significantly more than 9.8 mg/g of R-Char. It indicated that one-step ammonification failed to improve CO<sub>2</sub> adsorption of rice husk char at lower adsorption temperature (30 °C), which was due to Si-rich protective layer on the outer epidermis of rice husk. It is not only disadvantageous to the formation of pore structure, but also the CO<sub>2</sub> adsorption [33]. However, when this Si-rich protective layer was removed by HF solution, it can be found that HF-N-Char owned the largest capacity of CO<sub>2</sub> adsorption at both temperatures: 77.9 mg/g at 30 °C, and 18.1 mg/g at 120 °C. These results illuminated that the HF pre-deashing treatment of precursor did improve the CO<sub>2</sub> adsorption characteristics of nitrogen-enriched biochar. The reason of this phenomenon is probably that the HF pre-deashing of precursor not only removed the Si-rich structure, but also made three major components of rice husk (cellulose, lignin and hemicelluloses) separated [29]. These changes promoted the

**Table 5**  
EDX elements microanalysis for the sample surface, at 10  $\mu\text{m}$ .

Sample	Element (wt.%)											
	C <sup>s</sup>	N <sup>s</sup>	O <sup>s</sup>	Mg <sup>s</sup>	Al <sup>s</sup>	Si <sup>s</sup>	P <sup>s</sup>	S <sup>s</sup>	Cl <sup>s</sup>	K <sup>s</sup>	Ca <sup>s</sup>	Mn <sup>s</sup>
RH	18.80	2.28	33.86	0.05	—	43.71	1.30	—	—	—	—	—
HF-RH	56.41	3.20	38.53	0.17	0.14	0.19	0.07	0.21	0.15	0.18	0.33	0.42
HF-N-Char	89.95	5.03	4.27	0.10	0.04	0.07	0.06	0.10	—	—	0.23	0.14

<sup>s</sup>Surface element.

**Table 6**  
Surface atomic ratio of the sample surface, at 10  $\mu\text{m}$ .

Sample	C <sup>a</sup> (at.%)	N <sup>a</sup> (at.%)	O <sup>a</sup> (at.%)	Si <sup>a</sup> (at.%)	N <sup>a</sup> /C <sup>a</sup>	O <sup>a</sup> /C <sup>a</sup>	Si <sup>a</sup> /C <sup>a</sup>
RH	28.75	2.99	38.87	28.58	0.10	1.35	0.99
HF-RH	63.59	3.09	32.61	0.09	0.05	0.51	0.0014
HF-N-Char	92.04	4.42	3.28	0.03	0.05	0.04	0.0003

<sup>a</sup>Surface atomic.

development of pore structures, introduction of surface nitrogen functional groups and the increase of the surface activity, which enhanced physical adsorption as well as chemical adsorption [34].

The cyclic adsorption performance of R-char, N-Char, and HF-N-Char was effective at 30 °C, but deteriorated slightly at 120 °C with

cycle times. (About a 10% reduction was found for the third adsorption–desorption circle.) Essentially, biochars adsorb CO<sub>2</sub> better at 30 °C than that at 120 °C. The reason for this is that the CO<sub>2</sub> adsorption capacity at 30 °C is mainly attributed to physical adsorption, but chemical adsorption dominates at 120 °C – higher adsorption temperature drives down the regeneration of chemical adsorption active sites [7].

#### 4. Conclusion

This study investigated the effects of pre-deashing treatment on the physicochemical properties and CO<sub>2</sub> adsorption performance of

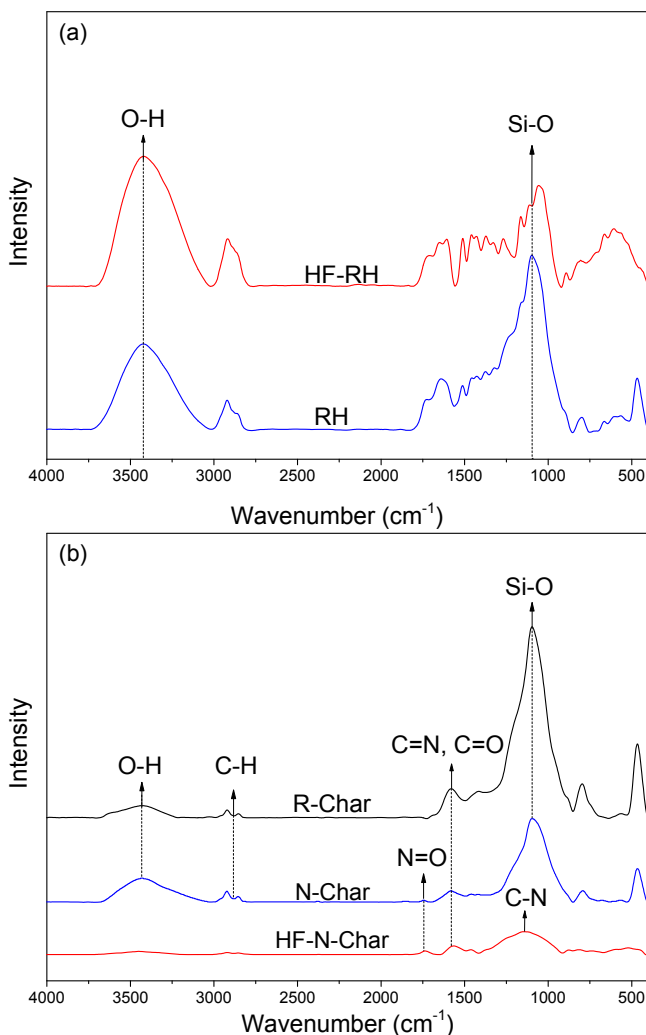


**Fig. 6.** FTIR spectra of rice husk (a) and chars (b).

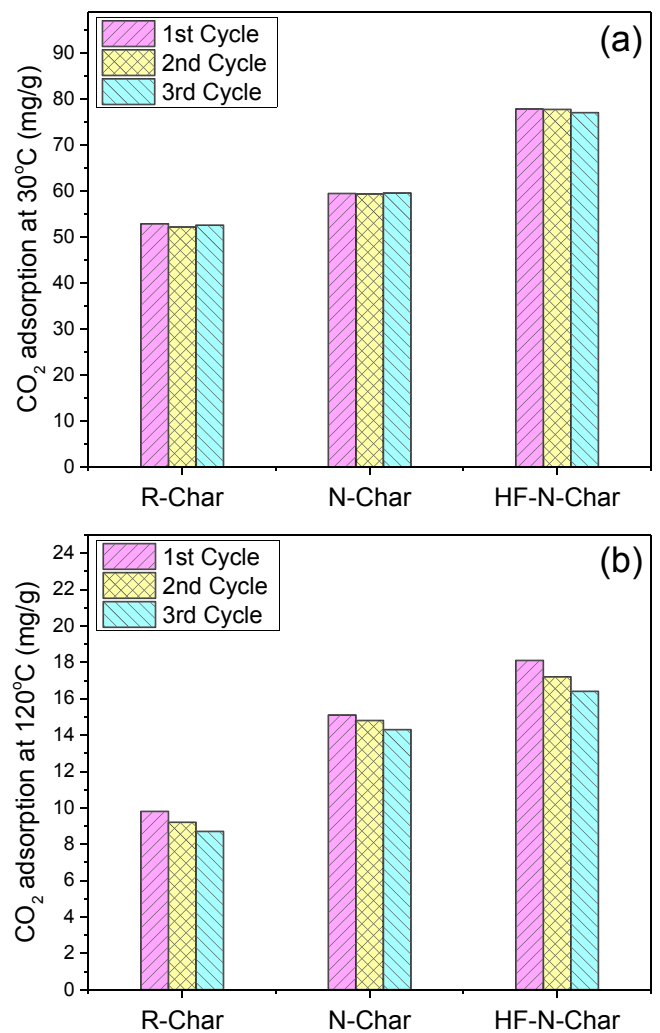


**Fig. 7.** CO<sub>2</sub> adsorption capacity in three adsorption–desorption cycles. CO<sub>2</sub> adsorption is conducted at 30 °C (a) and 120 °C (b). CO<sub>2</sub> desorption is conducted at 200 °C in N<sub>2</sub> atmosphere.

nitrogen-enriched rice husk biochar. The most notable conclusions are summarized as follows:

- (1) Deashing by HF solution destroys C–O–Si bonding in rice husk and removes the majority of Si content. Though N and O can be partially removed from rice husk during this process, the surface N and O content increases after deashing.
- (2) Deashing by HF solution deteriorates the original pore structures of rice husk, and removes the protective layer structure of the outer epidermis, but does benefit the physicochemical properties of the material (as evidenced by the HF-N-Char sample.) The  $S_{BET}$ ,  $S_{mic}$ ,  $V_{mic}$  and total N content of HF-N-Char all increased significantly.
- (3) The introduction of N-containing functional groups during ammonification influences the pore size distribution of biochars. Narrow mesopores (2–7 nm) are blocked, while micro- and macropores increase after ammonification.
- (4) The CO<sub>2</sub> adsorption capacity of HF-N-Char was 77.9 mg/g at 30 °C and 18.1 mg/g at 120 °C, while that of N-Char was 59.6 mg/g at 30 °C and 15.1 mg/g at 120 °C. These results demonstrate that pre-deashing of rice husk by HF solution enhances both physical and chemical adsorption capacities of derived nitrogen-enriched biochars.

#### Acknowledgments

The authors wish to express their sincere thanks for the financial support from the National Basic Research Program of China (2013CB228102), the National Natural Science Foundation of China (51276075 and 51376076), and the Innovation Foundation of Huazhong University of Science and Technology (2014TS118 and CX14-035). The study also benefited from the technical support of the Analytical and Testing Center of Huazhong University of Science and Technology (<http://atc.hust.edu.cn>).

#### References

- [1] Hofmann DJ, Butler JH, Tans PP. A new look at atmospheric carbon dioxide. *Atmos Environ* 2009;43(12):2084–6.
- [2] Pachauri RK, Reisinger A. Climate change 2007 synthesis report: summary for policymakers: IPCC secretariat. 2007. [http://www.ipcc.ch/publications\\_and\\_data/ar4/syr/en/contents.html](http://www.ipcc.ch/publications_and_data/ar4/syr/en/contents.html).
- [3] Markewitz P, Kuckshinrichs W, Leitner W, Linssen J, Zapp P, Bongartz R, et al. Worldwide innovations in the development of carbon capture technologies and the utilization of CO<sub>2</sub>. *Energy Environ Sci* 2012;5(6):7281–305.
- [4] Pfaff I, Oexmann J, Kather A. Optimised integration of post-combustion CO<sub>2</sub> capture process in greenfield power plants. *Energy* 2010;35(10):4030–41.
- [5] Sun N, Sun C, Liu J, Liu H, Snape CE, Li K, et al. Surface-modified spherical activated carbon materials for pre-combustion carbon dioxide capture. *RSC Adv* 2015;5(42):33681–90.
- [6] Pevida C, Plaza MG, Arias B, Feroso J, Rubiera F, Pis JJ. Surface modification of activated carbons for CO<sub>2</sub> capture. *Appl Surf Sci* 2008;254(22):7165–72.
- [7] Plaza MG, Pevida C, Arenillas A, Rubiera F, Pis JJ. CO<sub>2</sub> capture by adsorption with nitrogen enriched carbons. *Fuel* 2007;86(14):2204–12.
- [8] Przepiórski J, Skrodzewicz M, Morawski AW. High temperature ammonia treatment of activated carbon for enhancement of CO<sub>2</sub> adsorption. *Appl Surf Sci* 2004;225(1–4):235–42.
- [9] Shafeeyan MS, Daud WMAW, Houshmand A, Shamiri A. A review on surface modification of activated carbon for carbon dioxide adsorption. *J Anal Appl Pyrol* 2010;89(2):143–51.
- [10] Jimenez V, Ramirez-Lucas A, Diaz JA, Sanchez P, Romero A. CO<sub>2</sub> capture in different carbon materials. *Environ Sci Technol* 2012;46(13):7407–14.
- [11] Rochelle GT. Amine scrubbing for CO<sub>2</sub> capture. *Science* 2009;325:1652–4.
- [12] Kwak N-S, Lee JH, Lee IY, Jang KR, Shim J-G. A study of the CO<sub>2</sub> capture pilot plant by amine absorption. *Energy* 2012;47(1):41–6.
- [13] Aaron D, Tsouris C. Separation of CO<sub>2</sub> from flue gas: a review. *Sep Sci Technol* 2005;40(1–3):321–48.
- [14] Zhang ZE, Yan YF, Zhang L, Ju SX. Hollow fiber membrane contactor absorption of CO<sub>2</sub> from the flue gas: review and perspective. *Glob Nest J* 2014;16:355–74.
- [15] Bounaceur R, Lape N, Roizard D, Vallieres C, Favre E. Membrane processes for post-combustion carbon dioxide capture: a parametric study. *Energy* 2006;31(14):2556–70.
- [16] Heidari A, Younesi H, Rashidi A, Ghoreyshi AA. Evaluation of CO<sub>2</sub> adsorption with eucalyptus wood based activated carbon modified by ammonia solution through heat treatment. *Chem Eng J* 2014;254:503–13.
- [17] Daud WMAW, Houshmand AH. Textural characteristics, surface chemistry and oxidation of activated carbon. *J Nat Gas Chem* 2010;19(3):267–79.
- [18] Ioannidou O, Zabaniotou A. Agricultural residues as precursors for activated carbon production—A review. *Renew Sust Energ Rev* 2007;11(9):1966–2005.
- [19] Raynal L, Bouillon P-A, Gomez A, Broutin P. From MEA to demixing solvents and future steps, a roadmap for lowering the cost of post-combustion carbon capture. *Chem Eng J* 2011;171(3):742–52.
- [20] Plaza MG, Pevida C, Martín CF, Feroso J, Pis JJ, Rubiera F. Developing almond shell-derived activated carbons as CO<sub>2</sub> adsorbents. *Sep Purif Technol* 2010;71(1):102–6.
- [21] Li B, Lei Z, Huang Z. Surface-treated activated carbon for removal of aromatic compounds from water. *Chem Eng Technol* 2009;32(5):763–70.
- [22] Yang H, Yuan Y, Tsang SCE. Nitrogen-enriched carbonaceous materials with hierarchical micro-mesopore structures for efficient CO<sub>2</sub> capture. *Chem Eng J* 2012;185–186:374–9.
- [23] Zhang X, Zhang S, Yang H, Feng Y, Chen Y, Wang X, et al. Nitrogen enriched biochar modified by high temperature CO<sub>2</sub>-ammonia treatment: characterization and adsorption of CO<sub>2</sub>. *Chem Eng J* 2014;257:20–7.
- [24] Das P, Ganesh A, Wangikar P. Influence of pretreatment for deashing of sugarcane bagasse on pyrolysis products. *Biomass Bioenergy* 2004;27(5):445–57.
- [25] Basta AH, Fierro V, Saied H, Celzard A. Effect of deashing rice straws on their derived activated carbons produced by phosphoric acid activation. *Biomass Bioenergy* 2011;35(5):1954–9.
- [26] Dombrowski RJ, Hyduke DR, Lastoskie CM. Pore size analysis of activated carbons from argon and nitrogen porosimetry using density functional theory. *Langmuir* 2000;16(11):5041–50.
- [27] Lua AC, Lau FY, Guo J. Influence of pyrolysis conditions on pore development of oil-palm-shell activated carbons. *J Anal Appl Pyrol* 2006;76(1–2):96–102.
- [28] Guo Q, Tian J. Removal of fluoride and arsenate from aqueous solution by hydrocalumite via precipitation and anion exchange. *Chem Eng J* 2013;231:121–31.
- [29] Park B-D, Wi SG, Lee KH, Singh AP, Yoon T-H, Kim YS. Characterization of anatomical features and silica distribution in rice husk using microscopic and micro-analytical techniques. *Biomass Bioenergy* 2003;25(3):319–27.
- [30] Ahmad F, Daud WMAW, Ahmad MA, Radzi R. The effects of acid leaching on porosity and surface functional groups of cocoa (theobroma cacao)-shell based activated carbon. *Chem Eng Res Des* 2013;91(6):1028–38.
- [31] McEnaney B. Adsorption and structure in microporous carbons. *Carbon* 1988;26(3):267–74.
- [32] Shafeeyan MS, Daud WMAW, Houshmand A, Arami-Niya A. Ammonia modification of activated carbon to enhance carbon dioxide adsorption: effect of pre-oxidation. *Appl Surf Sci* 2011;257(9):3936–42.
- [33] Yin G, Liu Z, Liu Q, Wu W. The role of different properties of activated carbon in CO<sub>2</sub> adsorption. *Chem Eng J* 2013;230:133–40.
- [34] Shen W, Fan W. Nitrogen-containing porous carbons: synthesis and application. *J Mater Chem A* 2013;1(4):999–1013.